JOURNAL OF SOLID STATE CHEMISTRY **130,** 58–65 (1997)
ARTICLE NO. SC977277

Structural and Bonding Trends in Tin Pyrochlore Oxides

Brendan J. Kennedy

School of Chemistry F11, The University of Sydney, Sydney, New South Wales 2006, Australia

and

Brett A. Hunter and Christopher J. Howard

Australian Nuclear Science and Technology Organisation, Private Mail Bag 1 Menai, New South Wales 2234, Australia

Received August 30, 1996; in revised form January 3, 1997; accepted January 8, 1997

The structures of a number of pyrochlore stannates of the type $Ln_2Sn_2O_7$, with *Ln* = Y, La, Pr, Nd, Tb–Lu and *Ln* = Sm, Eu, and Gd, have been refined by Rietveld analysis from 1.4925 Å neutron powder and 1.0 Å X-ray powder diffraction data, respectively. The single variable oxygen positional parameter is observed to decrease systematically with the increasing lattice parameter, causing periodic shifts in both the Sn–O and Sn–O–Sn interactions. The *Ln* temperature factors are highly anisotropic, and this is explained in terms of the stereochemistry of the *Ln* atoms. Bond valence sum calculations of the materials have been performed to explore changes in the bonding resulting from the structural changes. © 1997 Academic Press

INTRODUCTION

The cubic pyrochlore structure is adopted by a large number of complex oxides with the formula $A_2M_2O_7$ where A is a 2^+ or 3^+ ion and M is a 5^+ or 4^+ ion. Pyrochlore oxides are of interest as a consequence of their catalytic activity for a variety of processes (1) and high-temperature stability. Of the various pyrochlore oxides the stannates, $Ln_2Sn_2O_7$ (Ln = Y, La–Lu), form a very complete series of isostructural compounds and consequently have been well studied (2, 3). Recent interest in the stannate pyrochlores has stemmed from their high efficiency for the oxidative coupling of methane and their potential use as high-temperature gas sensors or fast ion conductors. The predisposition of pyrochlores toward defect structures is believed to be important for these applications. Stannate pyrochlores have been used as model compounds in magic angle spinning NMR studies of paramagnetic solids (3). There is also intense interest in ruthenium pyrochlore catalysts some of which exhibit a compositional dependent metal–semiconductor transition (4–6).

For the ruthenium pyrochlores it has been proposed that the Ru–O–Ru contact is important in determining the conductivity of the material, yet there appears to be little precise structural information on how this contact varies with the lanthanide. Previous structural studies of pyrochlores have indicated that the single variable oxygen positional parameter, x, increases, albeit rather erratically, as the lanthanide ionic radius decreases (1, 2). Mössbauer data on ^{119}Sn in the $Ln_2Sn_2O_7$ compounds were reported by Belyaev *et al.* (7) and Loeberstein *et al.* (8) and showed a systematic increase in the quadrupole splitting as the size of the unit cell increased. This suggests that the Sn^{4+} ion environment becomes less symmetrical as the cell size increases, presumably as a consequence of a systematic variation in the oxygen positional parameter. It has not yet been established if the oxygen positional parameter is governed primarily by the size of the trivalent ion or if other factors are important.

The cubic pyrochlore structure, space group $Fd3m$, has eight molecules of the general formula $A_2B_2O_6O'$ in the unit cell (Fig. 1). The *Ln* cations, occupying the 16*d* *A* sites, are coordinated to eight oxygen atoms placed at the vertices of a scalenohedron. This is axially compressed, with the two axial oxygen atoms (the O′ atoms at the 8*b* site) being at a slightly shorter distance from the central cation than the other six. The smaller Sn cations occupy the 16*c* *B* sites and are coordinated to six oxygen atoms at equal distances in trigonal antiprisms. The O atoms (on the 48*f* site) are at $(x, 0.125, 0.125)$ and are bonded to two *Ln* and two Sn atoms. The O′ atom is bonded only to the *Ln* atoms. Although the shorter *Ln*–O′ distance depends only on a $(= a\sqrt{3/8})$, the Sn–O and *Ln*–O distances depend on both the lattice parameter and the variable oxygen positional parameter.

The oxygen positional parameter can be obtained from refinement of powder diffraction data although, since O is a much weaker scatterer of X rays than either *Ln* or Sn,

0022-4596/97 $25.00
Copyright © 1997 by Academic Press
All rights of reproduction in any form reserved.

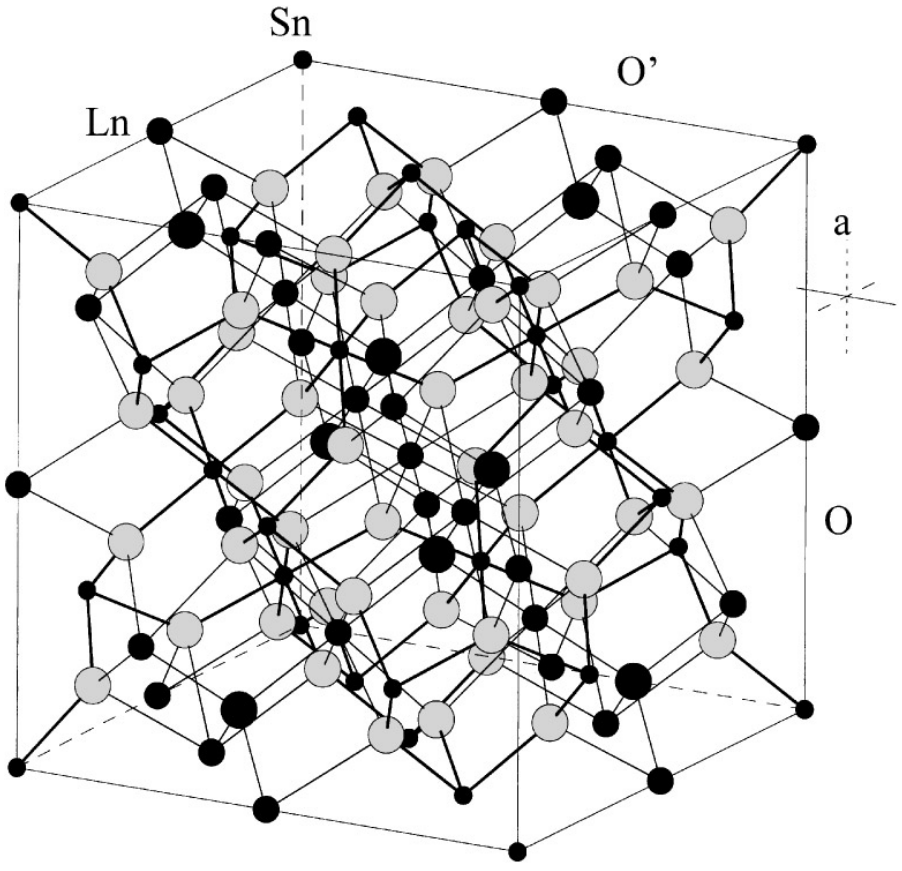

FIG. 1. View of the pyrochlore structure.

X-ray methods are of limited accuracy. Consequently, powder neutron diffraction methods have been used in the present study where possible. For Sm, Eu, and Gd, the high neutron absorption cross section precluded the use of neutron diffraction; consequently less accurate X-ray measurements were utilized. No Pm oxides were available for this work.

The major aims of the present work were to measure the oxygen positional parameter in the tin pyrochlore oxides and to examine the factors which determine its variation. The dependence of the Sn–O–Sn angle on the lattice parameter allows a comparison with other pyrochlores, in particular the metallic ruthenium and iridium pyrochlores. A secondary aim was to characterize the anisotropic thermal displacements of the materials and, if possible, understand the stereochemical influences on these motions.

EXPERIMENTAL AND DATA ANALYSIS

Polycrystalline samples of the stannate pyrochlores were prepared by the solid state reaction of SnO_2 with the appropriate lanthanum or yttrium oxide. The finely ground samples were heated at 1000°C for 2 days and then at 1400–1500°C for 5 days, with intermediate regrinding, or until powder X-ray diffraction measurements did not show the presence of any material other than the desired pyrochlore.

The powder neutron diffraction patterns were collected at room temperature using neutrons of wavelength 1.4925 Å in 0.05° steps on the eight counter high-resolution powder diffractometer (HRPD) at the Australian Nuclear Science and Technology Organisation's HIFAR reactor (9). Approximately 10–15 g of each sample was loaded into a 12- or 16-mm vanadium can which was slowly rotated during the measurement to minimize the effects of preferred orientation. Where necessary the data were corrected for the effects of absorption.

Preliminary powder X-ray diffraction measurements were performed on a Siemens D5000 diffractometer using Cu$K\alpha$ radiation, and high-resolution data were collected at room temperature using synchrotron radiation of wavelength 1.00 Å in 0.01° steps at the Australian National Beamline Facility, Beamline 20B, at the Photon Factory, Japan (10). For these measurements the diffractometer was operated in $\theta - 2\theta$ mode and the flat plate sample was rotated throughout the measurements.

Least-squares structure refinements were performed with a PC version of the Rietveld analysis program LHPM (11). The calculated intensities assume a Voigt function profile, where the width of the Gaussian component varies in accordance with the Caglioti, Paoletti, and Ricci function and the Lorentzian component width varies with $\sec\theta$. The background was defined by a third-order polynomial in 2θ and was refined simultaneously with the other profile and structural parameters. Refinements were continued until the parameter shifts in the last cycle were less than 10% of their associated e.s.d.'s. Further details are given in Table 1.

Bond valence sums were determined using the program EUTAX (12). These sums were obtained by first determining bond valences as

$$v_{ij} = \exp[(R_0 - d_{ij})/0.37] ,$$

where values for R_0 are the bond valence parameters for each bond pair taken from Brown and Altermatt (13) and d_{ij} are the measured bond lengths. Bond valence sums were then obtained by simply summing over all neighbors for each site:

$$V_i = \sum v_{ij} .$$

RESULTS

Structure

The final atomic coordinates and temperature factors obtained by Rietveld refinement from powder neutron diffraction data for the series of 11 pyrochlore stannates studied are given in Table 1, and the corresponding data obtained for the Sm, Eu, and Gd stannates by powder XRD methods are given in Table 2. Figure 2a shows a typical plot of observed, calculated, and difference profiles for the Rietveld refinements from the neutron diffraction data and Fig. 2b shows a corresponding plot from an X-ray diffraction pattern. In all cases, the agreement between the observed and calculated profiles is excellent. The values obtained for the cubic lattice parameters are in agreement with the values obtained earlier by Brisse and Knop (2) and, as was also found in their work, the cubic lattice parameter displays

TABLE 1
Room Temperature Structural and Temperature Parameters (10^{-3} Å^2) for Some Stannate Pyrochlores Obtained from a Rietveld-Type Refinement from Powder Neutron Diffraction Data

	Y	La	Pr	Nd	Tb	Dy	Ho	Er	Tm	Yb	Lu
Ionic radii (Å)	0.90	1.03	0.99	0.98	0.92	0.91	0.90	0.89	0.88	0.87	0.86
a (Å)	10.3723(1)	10.7026(1)	10.6004(1)	10.5671(1)	10.4235(2)	10.3979(3)	10.3726(2)	10.3504(1)	10.3262(2)	10.3046(1)	10.2917(2)
x (O)	0.33694(5)	0.32943(7)	0.33148(5)	0.33220(9)	0.3356(1)	0.3372(3)	0.3366(1)	0.3375(1)	0.3382(1)	0.33908(7)	0.3397(1)
Anisotropic thermals											
Ln											
$U_{11} = U_{22} = U_{33}$	5.4(2)	4.5(2)	5.1(2)	5.2(2)	6.2(3)	4.4(3)	6.7(3)	3.4(3)	7.3(4)	6.4(1)	9.7(4)
$U_{12} = U_{13} = U_{23}$	− 0.9(2)	− 0.9(2)	− 0.6(3)	− 1.0(5)	− 0.8(3)	− 0.1(1)	− 0.2(4)	− 1.2(3)	− 0.2(4)	− 1.3(2)	0.4(6)
Sn											
$U_{11} = U_{22} = U_{33}$	2.7(2)	2.7(2)	2.9(2)	5.2(2)	5.5(3)	3.2(7)	7.1(4)	1.3(3)	5.0(4)	2.9(2)	7.0(4)
$U_{12} = U_{13} = U_{23}$	− 0.3(2)	− 0.2(3)	− 0.1(2)	0.0(4)	− 0.1(5)	− 0.3(9)	0.7(5)	0.0(1)	0.3(6)	− 0.7(3)	0.4(6)
O											
U_{11}	6.4(3)	6.0(3)	6.2(2)	8.9(4)	9.3(5)	6.1(1.2)	11.5(6)	5.0(5)	10.0(6)	8.6(4)	13.2(6)
$U_{22} = U_{33}$	5.6(2)	5.1(2)	5.9(1)	7.3(3)	7.3(3)	6.8(7)	10.1(4)	3.6(3)	8.1(4)	7.5(2)	12.1(4)
U_{23}	2.3(2)	2.1(3)	2.2(2)	2.0(3)	2.3(4)	2.2(8)	1.7(4)	2.2(8)	2.2(4)	2.6(3)	3.2(5)
O′											
$U_{11} = U_{22} = U_{33}$	4.9(4)	5.3(5)	5.5(3)	8.7(6)	9.9(8)	7.3(1.4)	7.2(8)	4.0(8)	7.1(9)	7.6(5)	10.0(1.0)
Selected contacts											
Sn–O (Å)	2.043	2.074	2.063	2.060	2.047	2.050	2.042	2.042	2.040	2.0398	2.0401
Ln–O (Å)	2.495	2.629	2.589	2.576	2.516	2.499	2.497	2.485	2.475	2.4633	2.4559
Ln–O′ (Å)	2.246	2.317	2.295	2.288	2.257	2.251	2.246	2.2401	2.236	2.2310	2.2282
Sn–O–Sn (°)	127.62	131.61	130.51	130.12	128.32	127.48	127.80	127.33	126.97	126.51	126.19
Ln–O–*Ln* (°)	94.62	92.05	92.74	92.98	94.16	94.71	94.50	94.82	95.07	95.38	95.60
O–Sn–O (°)	99.06	96.47	97.19	97.45	98.61	99.10	98.94	99.24	99.48	99.76	99.96
R_p (%)	4.1	4.96	3.90	5.27	6.05	6.38	6.00	5.35	5.86	3.88	5.94
R_{wp} (%)	5.5	6.50	4.76	6.81	7.29	7.46	7.00	6.25	7.17	4.93	7.78
R_{exp} (%)	3.9	4.54	3.29	4.77	4.43	6.67	4.39	5.11	4.95	2.83	5.25
R_{bragg} (%)	0.60	0.70	0.77	1.47	2.71	2.49	3.14	1.36	1.93	1.47	1.99

TABLE 2
Room Temperature Structural and Temperature Parameters for Some Stannate Pyrochlores Obtained from a Rietveld-Type Refinement from Powder X-Ray Diffraction Data

	Gd	Eu	Sm
Ionic radii (Å)	0.94	0.95	0.96
a (Å)	10.45438(3)	10.47526(3)	10.51005(2)
x (O)	0.3348(9)	0.3338(10)	0.3330(6)
Isotropic thermals			
Ln	0.44(2)	0.41(1)	0.37(1)
Sn	0.32(2)	0.33(2)	0.22(6)
O(1)	0.9(2)	1.5(3)	0.6(1)
O′	0.8(5)	1.1(5)	0.6(3)
Selected contacts			
Sn–O (Å)	2.048	2.048	2.054
Ln–O (Å)	2.537	2.540	2.554
Ln–O′ (Å)	2.265	2.268	2.2756
Sn–O–Sn (°)	128.8	129.2	129.7
Ln–O–*Ln* (°)	98.3	98.1	97.8
R_p (%)	10.94	12.05	10.84
R_{wp} (%)	14.33	15.74	14.07
R_{exp} (%)	16.30	17.46	15.12
R_{bragg} (%)	2.33	2.58	3.09

a linear increase with increasing ionic radii of the lanthanides (Fig. 3) suggesting that these oxides are simple ionic compounds. There is no evidence for any substitution of Sn^{4+} onto the Ln^{3+} site in contrast to $Y_2Ti_2O_7$ where Y–Ti replacement occurs, albeit at a very low level (14), nor is there any evidence for anion disorder and/or nonstoichiometry. This latter observation is somewhat surprising since Chapman *et al.* (15) reported both $La_2Sn_2O_7$ and $Y_2Sn_2O_7$ to be semiconductors, where the carrier is believed to result from oxygen nonstoichiometry. Either these materials are susceptible to oxygen nonstoichiometry at higher temperatures, where the conductivity is greater, or the conduction is dominated by grain boundary and/or surface effects (16).

The variable oxygen positional parameter, x, varies from 0.3294 to 0.3397 over the series of stannate pyrochlores. Whereas literature reports (1, 2) suggest an irregular variation in x, we find (Fig. 4) there is an approximately linear relationship between x and the cubic lattice parameter a. The greatest deviation from a simple linear relationship occurs for the smallest cells. It has been suggested (17) that the pyrochlore structure will only be favored if the radius ratio r^{3+}/r^{4+} is in the range 1.46–1.80. Taking the radius of six-coordinate Sn^{4+} to be 0.69 Å (18) implies that the smaller lanthanides, Er–Lu, are at the edge of this stability domain. This instability can be rationalized in light of electrostatic energy calculations which suggest that the stability of the complexes decreases with increased x values (19). As discussed in more detail below, the increased deviation from linear behavior of the x vs a plot for the smaller cells appears to be due to compression of the Sn^{4+} cations and a compensating small displacement of the O atom at the 48*f* site leading to higher values of x. Also apparent from Fig. 4 is that the value of x for $Y_2Sn_2O_7$ (20) is greater than that for $Ho_2Sn_2O_7$ despite the similarity in the lattice parameters. Examination of the data suggests that the Ho compound is the anomalous result although it is unclear why this should be. The regular variation in x is in accord with the previously published ^{119}Sn Mossbauer data which show (7, 8) that the quadrupole splitting ΔE_q varies systematically with the cubic lattice parameter. The quadrupole splitting depends on the electric field gradient and is a measure of the departure of SnO_6 from a regular octahedron. For the SnO_6 polyhedron, being a trigonal antiprism stretched along the $\bar{3}$ axis, the value of ΔE_q is appreciable. As x is reduced this trigonal antiprism approaches a regular octahedron (it would become one at $x = 0.3125$) and ΔE_q is also reduced (7, 8).

As a consequence of the relationship between x and a the *Ln*–O and *Ln*–O′ distances show an approximate and strict linear dependence on a, respectively. However the Sn–O distance shows distinct curvature for the smaller lanthanides (Fig. 5). The apparent minimum Sn–O distance is about 2.040 Å. This distance compares with values of around 2.05–2.06 Å found in other Sn oxides such as rutile SnO_2 (21), perovskite $CaSnO_3$ (22), and ilmenite $MnSnO_3$ (23) and is among the shortest observed for six-coordinate Sn^{4+} oxides; it is smaller than the sum of the effective ionic radii (18) of 1.38 Å for four-coordinate O^{2-} and 0.69 Å for six-coordinate Sn^{4+}. In four-coordinate Sn^{4+}, shorter distances, of around 1.95 Å, are observed for example in Cs_4SnO_4 (24). These results demonstrate that for the smaller lanthanides there is considerable compression of the SnO_6 octahedron which is partially compensated by the increased x parameter. Alternatively if it is assumed that the value of $r_{O^{2-}}$ is correct, this implies the effective ionic radius of six coordinated Sn^{4+} is 0.66 Å.

Figure 6 illustrates the dependence of the O–Sn–O and Sn–O–Sn angles on the lattice parameter. The Sn–O–Sn angle generally decreases with decreased values of a (Fig. 6), but the relationship is nonlinear as a result of the increased displacement of the 48*f* site O at small a values. Although this observation is of limited importance for the nonmetallic stannate pyrochlores, it may have significance for the ruthenate and iridate pyrochlores, in which the *M*–O–*M* interactions are believed to be central in controlling the conductivity. The anomalously small values of *M*–O–*M* which have been reported (4) as being a critical feature for metallic conductivity in the ruthenate pyrochlores may in fact have a simple structural origin, as seen for example in $Lu_2Sn_2O_7$.

There is considerable anisotropy of the *Ln* temperature factors (Table 1). Although the values are relatively large,

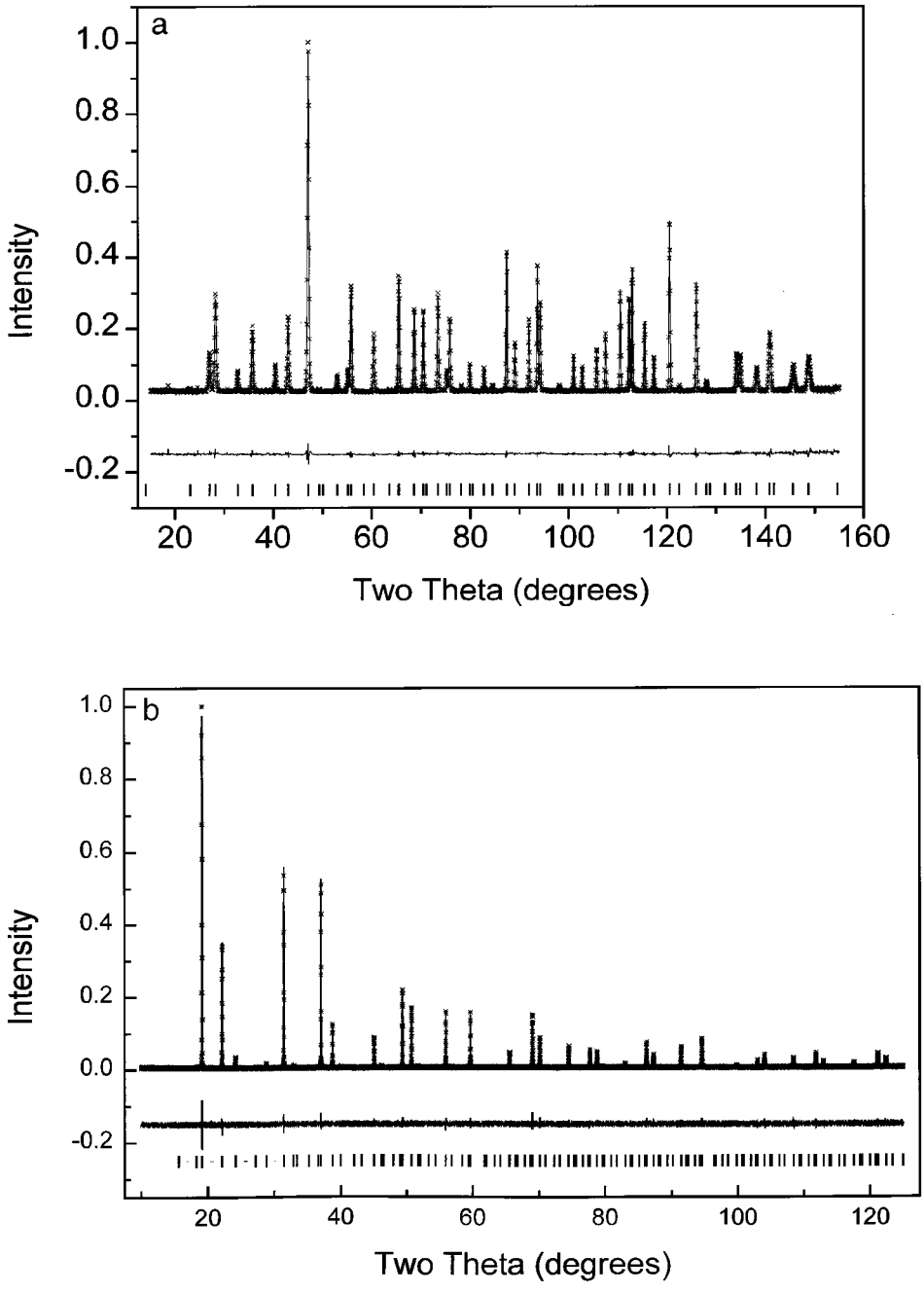

FIG. 2. (a) Observed, calculated, and difference neutron powder diffraction profiles for $Pr_2Sn_2O_7$. (b) Observed, calculated, and difference X-ray powder diffraction profiles for $Gd_2Sn_2O_7$. In both cases the observed data are indicated by crosses and the calculated profile by the solid line. The short vertical lines below the profiles mark the position of all possible Bragg reflections.

they are noticeably smaller than those found for $Cd_2Nb_2O_7$ where a temperature-dependent disorder of Cd from the 16*c* site appears to be present (25). There is no evidence for such disorder in the stannate pyrochlores. The *Ln* atoms lie on a threefold axis ($\bar{3}m$ site symmetry) and the thermal ellipsoid is one of rotation where the unique axis is the threefold axis. The principal mean-square atomic displacements of the *Ln* atoms are given by $U_{11} - U_{12}$, corresponding to motion perpendicular to the [111] direction, and $U_{11} + 2U_{12}$ parallel to the [111] direction, that is toward the two closest O′ atoms. In all cases the latter displacement is notably smaller. Similar behavior has been previously noted for the

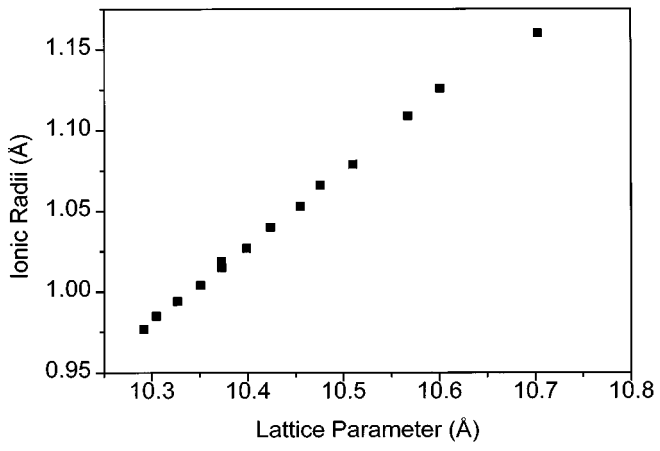

FIG. 3. Variation of the cubic lattice parameter with the ionic radii of the lanthanide in the series of stannate pyrochlores ($Ln_2Sn_2O_7$). Ionic radii taken from reference (18).

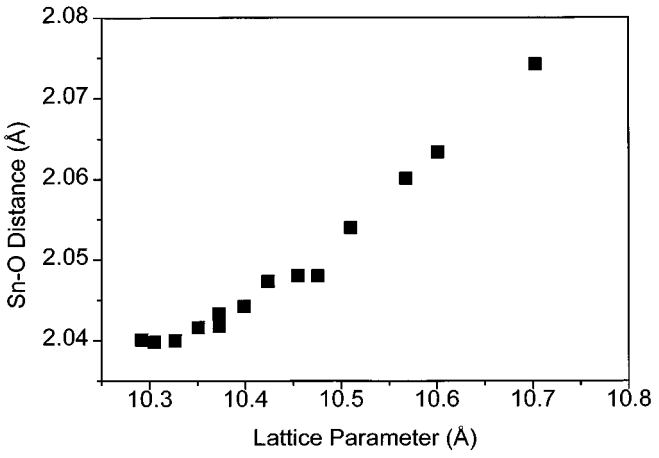

FIG. 5. Variation of the Sn–O bond distance with the cubic lattice parameter in $Ln_2Sn_2O_7$.

pyrochlore structure (26, 27). This result can be readily understood in terms of bond compression (20, 28), where the displacement of the *Ln* toward the O′ atoms is strongly inhibited. Bolzan and co-workers (21) showed that the mean-square atomic displacements of the oxygen atoms in rutile-type metal dioxides are dependent on the cell volume; it might be imagined that there should be a similar dependence for the *Ln* atom in the present oxides. That this is not observed demonstrates the importance of both bonding and nonbonding contacts in determining the magnitude of thermal displacement. For the oxygen atoms on the 48*f* site (C_{2v} site symmetry) having two nearest Sn and two more distant *Ln* neighbors the environment is also distorted. In this case movement along the Sn–O–Sn chains which is described by the principal vibration ($U_{22} - U_{23}$) corresponding to displacement in the $(0\bar{1}1)$ plane is always smaller than displacement in either the [100] or the [011] direction, given by U_{11} and ($U_{23} + U_{23}$), respectively.

Bonding

Figure 7 shows the variation in the bond valence sums (BVS) for the four ions present, namely, *Ln*, Sn, O, and O′. It is anticipated, from the variations in bond lengths and the reduction in the atomic volume, that there will be a systematic increase in the electron density at the Sn nuclei as *a* decreases. This is apparently confirmed by the BVS calculations for Sn which show a small increase as the lattice parameter and hence the cell volume contracts, i.e., as the Sn–O distance decreases. The decrease in V_{Sn} as the ionic radii of the lanthanides increase suggests an increasing level of covalency in Sn–O bonding. This increase is greatest for

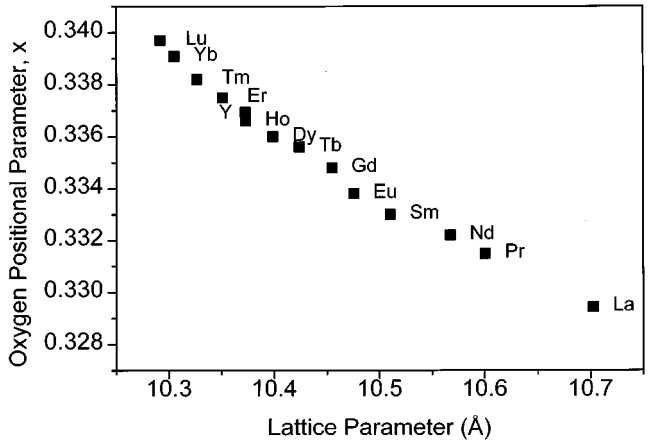

FIG. 4. Variation of the oxygen positional parameter, *x*, with the cubic lattice parameter for the series of stannate pyrochlores ($Ln_2Sn_2O_7$).

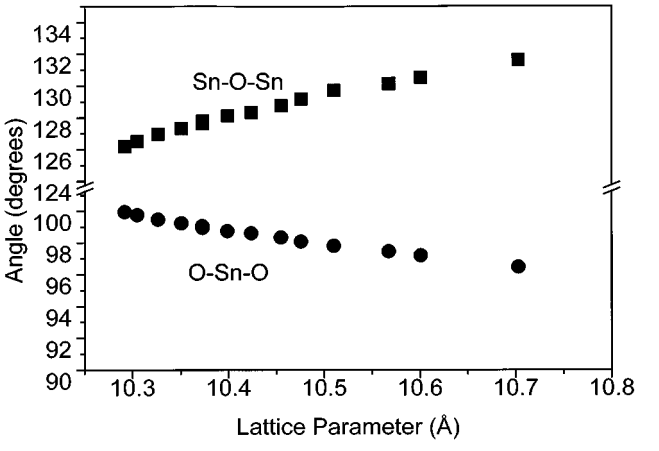

FIG. 6. Variation of the Sn–O–Sn and O–Sn–O bond angles with the cubic lattice parameter in $Ln_2Sn_2O_7$.

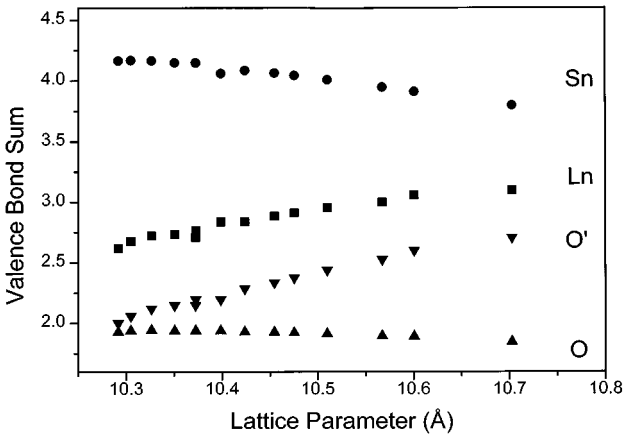

FIG. 7. Variation of the bond valence sums with the cubic lattice parameter in the series of stannate pyrochlores ($Ln_2Sn_2O_7$).

the larger lanthanides and especially La. Similarly, the small variation in V_O suggests a weaker covalent interaction. The variation in electron density at the Sn nuclei arising from the structural changes should be reflected in the isomer shifts obtained in the ^{119}Sn Mossbauer studies. Indeed in such studies it is found (7, 8) that the isomer shift is effectively constant over the series of pyrochlore stannates; previously this has been ascribed to the near constant Sn–O bond length seen for the series of pyrochlore stannates. However, the present work has demonstrated that there is a systematic variation in the Sn–O bond distance. So it would appear that additional factors are important, the most probable being a covalent interaction between the Sn and O which moderates the differences in the otherwise pure Sn–O ionic bonds. Independent evidence for covalency in the Sn–O bonding comes from a maximum entropy method analysis of X-ray diffraction data for $Y_2Sn_2O_7$ (29).

There is much greater variation in the BVS for the *Ln* ion. Here the BVS decreases from 3.095 in $La_2Sn_2O_7$ to 2.616 in $Lu_2Sn_2O_7$ indicative of considerable covalency. The BVS for O′, which forms the shortest Ln–O′ bond, also shows a significant variation, from 2.595 to 1.998 for the same pair of compounds. It is not surprising that the La–O′ interaction shows the strongest variations since this is the shortest bond distance. Fourquet *et al.* reported (30) significant variations in the BVS for Tl in the oxygen-deficient pyrochlore $Tl_2Nb_2O_{6+x}$ which are ascribed to covalent bonding by the easily polarizable Tl ions. Covalency in the harder Ln^{3+} ions is somewhat more surprising and worthy of additional study.

CONCLUSION

This is the first systematic study of the structural and bonding trends in a series of pyrochlore oxides which do not exhibit unusual electronic effects. There is a simple evolution of the structural features found in the stannate pyrochlores, although there appears to be a minimum in the Sn–O bond distance of 2.040 Å. Interestingly, BVS calculations indicate that covalent bonding interactions are important. The trends observed herein have been utilized as a basis to explore anomalies in the metallic ruthenate and iridate pyrochlores, results of which are reported elsewhere (31, 32).

ACKNOWLEDGMENTS

This work has been partially supported by the Australian Research Council, the Australian Institute of Nuclear Science and Engineering, and the Australian National Beamline Facility.

REFERENCES

1. M. A. Subramanian, G. Aravamudan, and G. V. Subba Rao, *Prog. Solid State Chem.* **15,** 55 (1983).
2. F. Brisse and O. Knop, *Can. J. Chem.* **46,** 857 (1968).
3. C. P. Grey, M. E. Smith, A. K. Cheetham, C. M. Dobson, and R. Dupree, *J. Am. Chem. Soc.* **112,** 4670 (1990), and references therein.
4. H. Kobayashi, R. Kanno, Y. Kawamoto, T. Kamiyama, F. Izumi, and A. W. Sleight, *J. Solid State Chem.* **114,** 15 (1995).
5. H. S. Jarrett, A. W. Sleight, J. F. Weiher, J. L. Gillson, C. G. Frederick, G. A. Jones, R. S. Swingle, D. Swatzfager, J. E. Gulley, and P. C. Hoell, *in* "Valence Instabilities and Related Narrow Band Phenomena" (R. D. Parks, Ed.), p. 545. Plenum, New York, 1977.
6. P. A. Cox, J. B. Goodenougth, P. J. Tavener, D. Telles, and R. G. Edgell., *J. Solid State Chem.* **62,** 360 (1986).
7. L. M. Belyaev, I. S. Lyubutin, L. N. Dem'yanets, T. V. Dmitieva, and L. P. Mitina, *Sov. Phys. Solid State* **11,** 424 (1969).
8. H. M. Loeberstein, R. Zilber, and H. Zmora, *Phys. Lett. A* **33,** 453 (1970).
9. C. J. Howard, C. J. Ball, R. L. Davis, and M. M. Elcombe, *Aust. J. Phys.* **36,** 507 (1983).
10. Z. Barnea, D. C. Creagh, T. J. Davis, R. F. Garrett, S. Jansky, A. W. Stevenson, and S. W. Wilkens., *Rev. Sci. Instrum.* **63,** 1069 (1992).
11. R. J. Hill and C. J. Howard, "Australian Atomic Energy Commission Report M112." AAEC (now ANSTO), Lucas Heights Research Laboratories, NSW, Australia, 1986.
12. M. O'Keeffe, "EUTAX, Version 1.3." Emlab Software, Phonix, AZ, 1993.
13. I. D. Brown and D. Altermatt, *Acta Crystallogr. B* **41,** 244 (1985).
14. C. Heremans, B. J. Wuensch, J. K. Staick, and E. Prince, *J. Solid State Chem.* **117,** 108 (1995).
15. R. A. Chapman, B. D. Meadowcroft, and J. Walkden, *J. Phys. D. Appl. Phys.* **3,** 307 (1970).
16. N. Wakiya, S. Nishiyama, K. Shinozaki, and N. Mizutani, *J. Solid State Chem.* **102,** 349 (1993).
17. F. Brisse, D. J. Stewart, V. Seidl, and O. Knop, *Can. J. Chem.* **50,** 3648 (1972).
18. R. D. Shannon, *Acta Crystallogr. A* **32,** 751 (1976).
19. J. Pannetier, *J. Phys. Chem. Solids* **34,** 583 (1973).
20. G. R. Facer, C. J. Howard, and B. J. Kennedy, *Powder Diff.* **8,** 245 (1993).
21. A. A. Bolzan, C. Fong, B. J. Kennedy, and C. J. Howard, *Acta Crystallogr. B* **53**.
22. A. Vagas, M. Vallet-Regi, J. M. Gonalez-Calbet, and M. A. Alario-Franco, *Acta Crystallogr. B* **42,** 167 (1986).
23. B. Durand, M. Diot, and P. Mollart, *Ann. Chim.* **4,** 599 (1979).

24. K. Bernet and R. Hoppe, *Z. Anorg. Allg. Chem.* **587,** 145 (1990).
25. K. Lukaszewicz, A. Pietraszko, J. Stepien-Damm, and N.N. Kolpakova, *Mater. Res. Bull.* **29,** 987 (1994).
26. A. W. Sleight, *Inorg. Chem.* **7,** 1704 (1968).
27. M. A. Subramanian, C. C. Torardi, D. C. Johnson, J. Pannetier, and A. W. Sleight, *J. Solid State Chem.* **72,** 24 (1988).
28. L. Pauling, *Acta Crystallogr. B* **36,** 761 (1980).
29. C. J. Howard, D. J. Cookson, B. J. Kennedy, T. Ikeda, M. Takata, and M. Sakata, *Acta Crystallogr. A* **52,** C349 (1996).
30. J. L. Fourquet, H. Duroy, and Ph. Lacorre, *J. Solid State Chem.* **114,** 575 (1995).
31. B. J. Kennedy and T. Vogt, *J. Solid State Chem.* **126,** 261 (1996).
32. Ismunandar, B. J. Kennedy, B. A. Hunter, and T. Vogt, submitted for publication.